



Contents lists available at ScienceDirect

Bioorganic & Medicinal Chemistry Letters

journal homepage: www.elsevier.com/locate/bmcl

Imidazo[1,5-*a*]pyrazines: Orally efficacious inhibitors of mTORC1 and mTORC2

Andrew P. Crew^{a,*}, Shripad V. Bhagwat^a, Hanqing Dong^a, Mark A. Bittner^b, Anna Chan^a, Xin Chen^a, Heather Coate^a, Andrew Cooke^b, Prafulla C. Gokhale^b, Ayako Honda^a, Meizhong Jin^a, Jennifer Kahler^a, Christine Mantis^b, Mark J. Mulvihill^a, Paula A. Tavares-Greco^a, Brian Volk^a, Jing Wang^a, Douglas S. Werner^a, Lee D. Arnold^a, Jonathan A. Pachter^a, Robert Wild^b, Neil W. Gibson^a

^a(OSI) Oncology, OSI Pharmaceuticals, Inc., 1 Bioscience Park Drive, Farmingdale, NY 11735, USA

^b(OSI) Oncology, OSI Pharmaceuticals, Inc., 2860 Wilderness Place, Boulder, CO 80301, USA

ARTICLE INFO

Article history:

Received 6 January 2011

Revised 27 January 2011

Accepted 31 January 2011

Available online 3 February 2011

Keywords:

mTOR

mTORC1

mTORC2

Imidazo[1,5-*a*]pyrazine

Oral inhibitor

ABSTRACT

The discovery and optimization of a series of imidazo[1,5-*a*]pyrazine inhibitors of mTOR is described. HTS hits were optimized for potency, selectivity and metabolic stability to provide the orally bioavailable proof of concept compound **4c** that demonstrated target inhibition in vivo and concomitant inhibition of tumor growth in an MDA-MB-231 xenograft model.

© 2011 Elsevier Ltd. All rights reserved.

The mammalian target of rapamycin (mTOR) is a 289 kDa serine/threonine protein kinase and a member of the PI3K-related kinase (PIKK) family that plays an important role in the PI3K/mTOR/AKT pathway to integrate both extracellular and intracellular signals and serve as a central regulator of cell metabolism, growth, proliferation and survival.¹ In mammalian cells, mTOR resides in at least two physically and functionally distinct signaling complexes, mTORC1 and mTORC2. mTORC1 directly phosphorylates S6 kinase 1 (S6K1 T389) and the eIF4E binding protein 1 (4E-BP1 S65/T70) through which growth and protein synthesis are respectively regulated.² The prototypical mTOR inhibitors based around the macrolide rapamycin ('rapalogs') have been shown to inhibit phosphorylation of S6K1 and 4E-BP1 through inhibition of mTORC1 and hence, mTORC1 is considered as a rapamycin-sensitive complex.³ mTORC2 also phosphorylates 4E-BP1 (T37/46), and is additionally involved in phosphorylation of Akt on S473, the activation of which drives cancer-related cellular responses such as cell growth and proliferation.⁴ Rapamycin and the rapalogs do not directly inhibit mTORC2.

In the past several years, significant effort has been devoted to the discovery of small molecule ATP-competitive mTOR inhibitors, which by virtue of the identity of the respective kinase domains, can interact with both mTOR complexes, with enhanced

consequences compared to those agents inhibiting mTORC1 only.^{5,6} The list of agents now identified as dual mTORC1/2 inhibitors includes PI-103,^{7a} BEZ-235,^{7b} AZD8055,^{7c} Torin1,^{7d} PP242,^{7e} WYE-125132^{7f}, INK-128^{7g} and our own dual inhibitor OSI-027, an imidazotriazine-based small molecule which is currently in phase-I clinical trials.⁸ Herein we describe our early medicinal and computational chemistry efforts to optimize the high throughput screening (HTS) hits, imidazo[1,5-*a*]pyrazin-8-amine **1a** and **1b**, focusing on the substitutions at C-1 and C-3 positions to drive potency and DMPK properties. Proof of concept compound **4c** was discovered as a potent and orally bioavailable inhibitor with in vivo efficacy in a mouse xenograft model, and became the starting point for multivariate optimization and the discovery of OSI-027.

Our efforts towards identifying dual mTORC1/2 inhibitors began with a high throughput screening campaign of the OSI compound library using human mTOR isolated from HeLa cell lysates in a chemiluminescence-based ELISA assay,⁹ monitoring phosphorylation of full-length 4E-BP1 at T37/46, the so-called rapamycin insensitive sites.^{6c} Compounds were screened at a concentration of 10 μM with 2-fold compression, and in order to identify robust starting points, a final ATP concentration of 100 μM was used.

Among the multiple chemotypes identified, imidazo[1,5-*a*]pyrazine hits **1a** and **1b** (Fig. 1) were selected for follow-up based on our previous and positive experiences with this bicyclic skeleton that culminated in the identification of the clinical dual IGF-1R/IR agent OSI-906.¹⁰ Cognizant of the IGF-1R activity

* Corresponding author. Tel.: +1 631 962 0600; fax: +1 631 845 5671.

E-mail address: acrew@osip.com (A.P. Crew).

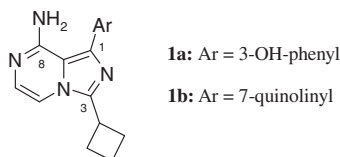


Figure 1. Representative imidazo[1,5-*a*]pyrazine HTS hits.

associated with this chemotype, we evaluated hits **1a** and **1b**, along with the known potent IGF-1R inhibitor **1c**,¹¹ in both mTOR and IGF-1R biochemical assays. As shown in Table 1, the phenol derivative **1a** exhibited activities for both targets. However, the 7-quinolinyl derivative **1b** demonstrated a preference for mTOR and in contrast, 2-phenyl-7-quinolinyl analog **1c** showed the a reverse preference suggesting that the hydrophobic pocket that productively accommodates the additional phenyl group in IGF-1R,¹¹ was either absent or topologically different in mTOR. This SAR observation indicated that the mTOR and IGF-1R activities of this series could be controlled through incorporation of appropriate substitution at the 1-position.

A variety of analogs at the C-1 position were prepared, including differently substituted phenyls and other bicyclic aryl groups, using the general synthetic routes described in our previous communication.¹² It was found that replacement of 3-hydroxyl group in compound **1a** with -NHAc, -NHSO₂Me, -NH₂, -CONH₂, -CH₂OH or its movement to the 4-position resulted in total loss of mTOR potency ($IC_{50} > 10 \mu\text{M}$). In contrast, the SAR of close analogs of quinoline **1b** was more productive (Table 2). Removal of the quinoline nitrogen (**1d**) afforded no appreciable change in potency, signifying that it played no significant part in binding to the protein. Its reposition to the 3-position (**1e**) or the addition of a second nitrogen to form a quinoxaline (**1f**) similarly had no effect on potency, neither did replacement of the distal ring with 5-membered nitrogen and sulphur heterocycles (**1i**, **1j** and **1k**). The 6-quinolinyl analog **1g** however, was approximately 8-fold less potent than the parent **1b**, and benzofuran **1l** was inactive, suggestive of an unfavorable electrostatic interaction between the heteroatom and the protein. Such effect in the case of the quinoxaline (**1f**) could be somewhat ameliorated by the second nitrogen in the bicyclic ring, possibly through electron-withdrawing effects. Repositioning of the naphthalene and indole attachment points (α -naphthenoid **1h** and 3-indole **1m**), resulted in a complete loss of activity. Replacement of the proximal ring with 5-membered heterocycles

Table 1
mTOR and IGF-1R potencies of compounds **1a–c**

Compd	Ar	IC_{50}^a (μM)	
		mTOR	IGF-1R
1a		1.97	0.52
1b		0.90	>10
1c		>9	0.08

^a Biochemical ELISA assay in the presence of 100 μM ATP; values are the mean of ≥ 2 experiments.

Table 2
SAR of different bicyclic aryl derivatives

Compd	Ar	IC_{50}^a (μM)	Compd	Ar	IC_{50}^a (μM)
1d		1.36	1k		1.30
1e		2.35	1l		>10
1f		2.60	1m		>10
1g		7.15	1n		0.46
1h		>10	1o		0.40
1i		2.48	1p		0.26
1j		3.12	1q		0.13

^a Biochemical ELISA assay in the presence of 100 μM ATP; values are the mean of ≥ 2 experiments

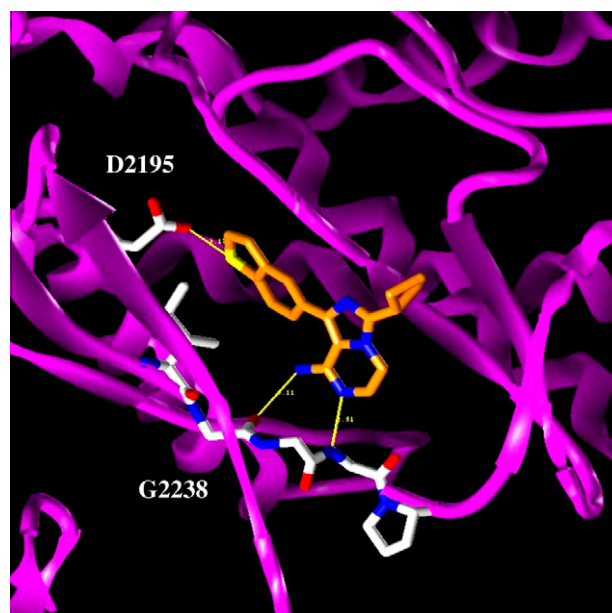


Figure 2. Binding of **1k** to the mTOR homology model.

Table 3

Deviations from co-planarity for the representative 6,6-, 6,5- and 5,6-bicyclic systems attaching to the 1-position

Compd	Ring system	α^a (°)
1d	6,6	-39.7
1h	6,6	-51.8
1i	6,5	-43.6
1j	6,5	-42.6
1n	5,6	-24.2
1o	5,6	-23.6
1p	5,6	0.3

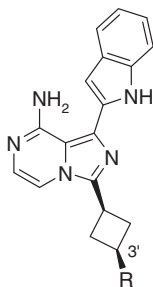
^a Torsional angle between the imidazopyrazine core and a 1-substituent after geometrical optimization of whole compound using ab initio method B3LYP and basis set 6-31G** (ref. Schrodinger Inc.).

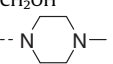
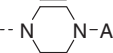
provided modest/good improvements in potency (e.g. **1n**, **1o**, **1p** and **1q**). By analogy with examples **1b** and **1d**, the additional nitrogen of azaindole **1o** offered no benefit over indole **1n**.

A homology model of the mTOR kinase was built based on the PI3K- γ and PI3K- γ crystal structures 1E8X and 2WXF, respectively. The complex modeling with compounds indicated that the imidazopyrazine derivatives fit the ATP-binding site with the 8-amino group and 7-nitrogen atom forming two hydrogen bonds with the backbone groups of Gly2238 and Val2240 considered to be the hinge residues of mTOR (Fig. 2), mimicking the binding mode of the purine ring in ATP. In addition, the model identified a number of pharmacophoric elements important for the binding of this chemotype to mTOR that helped the development and understanding of the associated SAR. (1) A narrow channel accommodates the C-1 aromatic substituent, and forces it to adopt an approximate coplanar conformation with respect to the imidazopyrazine core. This suggests why the 5,6-bicyclic systems (**1n**, **1o**, **1p** and **1q**) are generally more potent than the 6,6-bicyclic systems or 6,5-bicyclic systems, since the former systems have larger preferences toward the approximate co-planarity than the latter. Table 3 shows the results of ab initio geometrical calculations that support the increased torsional angle hypothesis for the 6,6 and 6,5 systems versus the 5,6 systems; (2) Asp2195 which is located at the end of the narrow channel destabilizes the binding

Table 4

SAR of imidazopyrazine-3-cyclobutyl derivatives



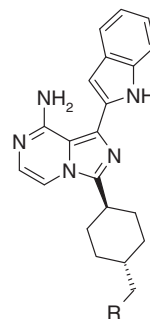
Compd	R	IC ₅₀ ^a (μM)	ER ^b	
			Mouse	Human
1n	H	0.46	0.94	0.92
2a	OH	0.37	0.60	0.74
2b	CH ₂ OH	0.32	0.79	0.70
2c		4.0	0.20	0.44
2d		0.35	0.59	0.58

^a Biochemical ELISA assay in the presence of 100 μM ATP; values are the mean of ≥ 2 experiments.

^b ERs determined with mouse and human liver microsomes.

Table 5

SAR of imidazopyrazine-3-cyclohexyl derivatives



Compd	R	IC ₅₀ ^a (μM)	ER ^b	
			Mouse	Human
3a	OH	0.22	0.67	0.74
3b	NH ₂	1.0	0.28	0.34
3c	NHAc	0.21	0.35	0.50
3d	NHCHO	0.15	0.51	0.64
3e	NHCO-cyclobutyl	0.17	0.79	0.74
3f	NHCO-3-furyl	0.09	0.76	0.78
3g	NHSO ₂ Me	0.41	ND	ND

ND = not determined.

^a Biochemical ELISA assay in the presence of 100 μM ATP; values are the mean of ≥ 2 experiments.

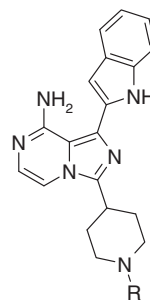
^b ERs determined with mouse and human liver microsomes.

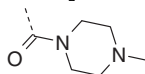
of compounds **1g** and **1l** by presenting repulsive electrostatic interactions to the nitrogen and oxygen atoms in the distal ring of the bicycle. In the case of **1g**, the increased Van der Waals contacts associated with the larger quinoline moiety partially offset the detrimental electronic effects to recover some potency unlike in the case of the benzofuran in **1l**. By comparison, Asp2195 stabilizes compound **1i** by forming a hydrogen bond with the indole NH moiety, and compound **1k** via a favorable oxygen-sulfur contact.

In line with previous observations on simple 3-cyclobutylimidazo[1,5-a]pyrazine derivatives,¹¹ the examples described in Table 2

Table 6

SAR of imidazopyrazine-3-piperidin-4-yl derivatives



Compd	R	IC ₅₀ ^a (μM)	ER ^b	
			Mouse	Human
4a	H	>10	0.64	0.18
4b	COMe	0.69	0.43	0.44
4c	CONMe ₂	0.12	0.67	0.68
4d		1.37	ND	ND

^a Biochemical ELISA assay in the presence of 100 μM ATP; values are the mean of ≥ 2 experiments.

^b ERs determined with mouse and human liver microsomes.

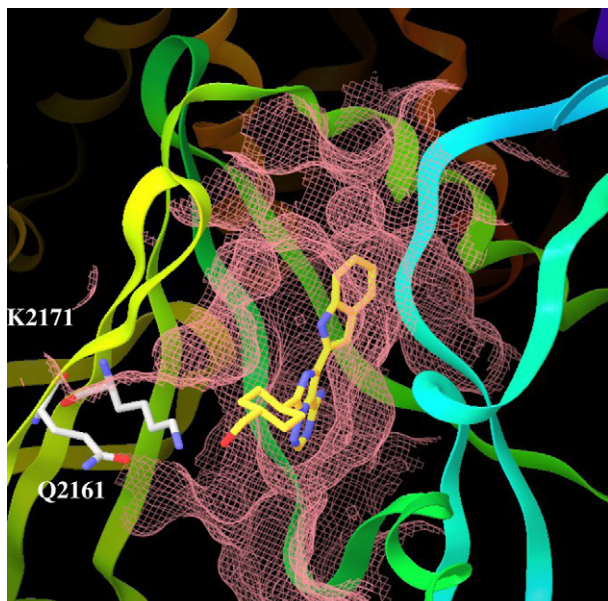


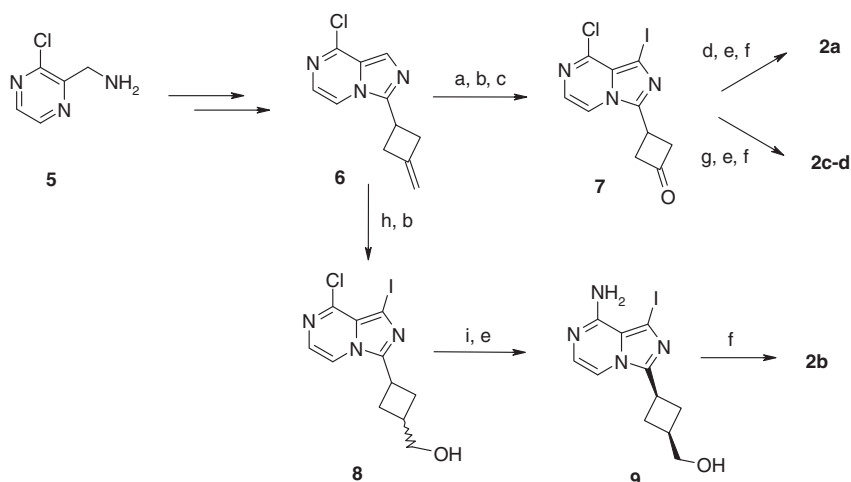
Figure 3. Binding of **3b** to the mTOR homology model.

exhibited poor in vitro metabolic stability with extraction ratios (ER) greater than 0.9, that is, predicting for >90% first-pass metabolism in vivo. Metabolic identification studies indicated that oxidation of the cyclobutyl ring at its unsubstituted distal position (3'-position in Table 4) was the primary liability of this system, therefore various modifications at this solvent-exposed region were pursued while maintaining the C-1 substituent as 2-indolyl (Tables 4–6).

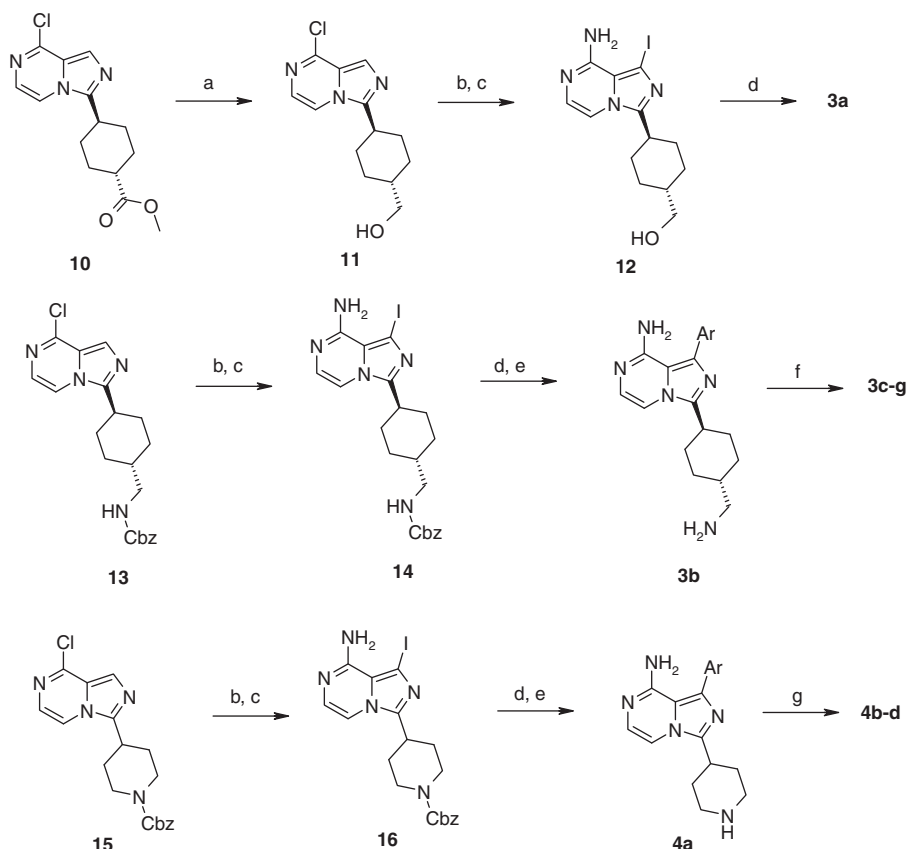
As shown in Table 4, substitutions at the cyclobutyl 3'-position had the desired effect on reducing ERs in both mouse and human liver microsomes. The hydroxyl (**2a**), hydroxymethyl (**2b**) and *N*-Ac piperazinyl (**2d**) derivatives were tolerated, however the basic *N*-Me piperazine derivative **2c** was significantly less active. Inspection of the mTOR homology model indicated that the cationic Lys2171 residue located in the proximity of the 3'-substituents, constituted a destabilizing factor for the compounds bearing a basic amino group. This unfavorable electronic effect was also observed for other compounds bearing a basic moiety (**3b**, **4a** and **4d**). On the other hand, Lys2171 offered a potential

hydrogen-bonding opportunity for some compounds, however, due to the desolvation penalties incurred in the binding processes, these hydrogen bonds appeared to contribute little gain to the binding energies (Fig. 3). The model also indicated that the imidazopyrazine 3-substituent was embraced by a large space with open access to the solvent that could accommodate both cyclobutyl and cyclohexyl systems. As shown in Tables 5 and 6, cyclohexyl and piperidine groups tethered to distal polar groups were well tolerated at the imidazopyrazine 3-position. Generally these polar groups could be used to modulate the overall physico-chemical properties and metabolic stability of the series without gross detriment to potency. In particular acetamide **3c** and urea **4c** offered a promising combination of sub-micromolar potency and moderate ERs, so these two agents were selected for further in vitro and in vivo profiling.

The syntheses of compounds **2a–d**, **3a–g** and **4a–d** shown in Tables 4–6 are described in Schemes 1 and 2. The bicyclic intermediate **6** was prepared by the amide coupling of 1-(3-chloropyrazin-2-yl)methylamine (**5**) with 3-methylidenecyclobutane-carboxylic acid followed by POCl₃-mediated cyclization.¹¹ Olefin **6** was converted to its diol derivative with NMO, and then iodinated at the 1-position followed by cleavage of the diol moiety with sodium periodate to afford ketone **7**. Reduction of **7** was achieved with sodium borohydride to stereo-specifically provide the *cis*-derivative, which was converted to compound **2a** through ammonolysis and a Suzuki coupling. Compounds **2c** and **2d** were prepared through the reductive amination of ketone **7** with the appropriate piperazine derivatives, again stereo-specifically affording the *cis*-products. The hydroboration of **6** was less selective however, producing a 5:1 mixture of *cis:trans* isomers that was inseparable by silica gel chromatography, as was the iodinated mixture **8**. Formation of a *p*-nitrobenzoate derivative allowed chromatographic isolation of pure *cis*-isomer. Upon ammonolysis at the 8-position, simultaneous deprotection of the benzoate ester was realized to give **9**, which was converted to compound **2b** through Suzuki chemistry. The syntheses of analogs **3a–g** and **4a–d** from intermediates **10**, **13** and **15** incorporated many of the same chemistries outlined for the cyclobutyl compounds in Scheme 1. In addition, the synthesis of **3a** involved a lithium aluminum hydride reduction of ester **10** to alcohol **11** that did not compromise the 8-chloro functionality and in fact was a quantitative conversion. The formation of the amine-derived compounds **3b–g** and **4a–d** also required extra steps for removal of the Cbz groups and subsequent final acylations.



Scheme 1. Preparation of compounds **2a–d**. Reagents and conditions: (a) NMO (50% w/w in water), cat. potassium osmate dihydrate, THF; (b) *N*-iodosuccinimide, DMF, 60 °C; (c) NaIO₄, THF–water (3:1, v/v), rt; (d) NaBH₄, MeOH–DCM (1:1, v/v), rt; (e) ammonia, 2-propanol, 110 °C, 24 h; (f) 2-(4,4,5,5-tetramethyl-1,3,2-dioxaborolan-2-yl)-1*H*-indole, PdCl₂(dppf), K₂CO₃, DME–water (4:1, v/v), 100 °C, 12 h; (g) NaBH(OAc)₃, amine, DCE, rt; (h) 9-BBN, THF, then NaBO₃·H₂O in water; (i) 4-nitrobenzoyl chloride, DIEA, DCM.



Scheme 2. Preparation of compounds **3a–g** and **4a–d**. Reagents and conditions: (Ar = 1*H*-indol-2-yl): (a) lithium aluminum hydride, THF, -78°C to rt; (b) *N*-iodosuccinimide, DMF, 60°C ; (c) ammonia, 2-propanol, 110°C , 24 h; (d) 2-(4,4,5,5-tetramethyl-1,3,2-dioxaborolan-2-yl)-1*H*-indole, $\text{PdCl}_2(\text{dppf})$, K_2CO_3 , DME–water (4:1, v/v), 100°C , 12 h; (e) concd HCl, rt, 12 h; (f) carboxylic acid, EDC, DIEA, DCM for **3c–f**; MeSO_2Cl , DIEA, DCM for **3g**; (g) HOAc, EDC, DIEA, DCM for **4b**; carbamoyl chloride, DIEA, DMF for **4c–d**.

Table 7
In vitro kinase selectivity of compounds **3c** and **4c**

Kinase ^a	3c	4c
mTOR	0.21	0.12
Abl	1.96	>10
EGFR	3.58	>10
cRaf	0.18	1.7
IGF-1R	2.72	>30
IR	22.6	>30
KDR	4.21	>10
MEK1	0.96	>10
PDK1	11.2	>30
PI3K γ	>30	>30
Src	5.30	0.77

^a Run in presence of 100 μM ATP.

Table 8
Mouse pharmacokinetic parameters for compounds **3c** and **4c**

Route of administration and parameters		3c	4c
iv	Dose (mg/kg)	1	5
	CL (mL/min/kg)	2	7
	$t_{1/2}$ (h)	1.6	0.9
	$\text{AUC}_{0-\infty}$ (ng h/mL)	6876	12092
	V_{ss} (L/kg)	0.2	0.4
p.o.	Dose (mg/kg)	20	20
	C_{max} (μM)	30.6	35.9
	$\text{AUC}_{0-\infty}$ (ng h/mL)	73824	49421
	F (%)	54	102

Further in vitro characterization of compounds **3c** and **4c** included an assessment of selectivity versus a small panel of kinases (Table 7). Both agents offered a reasonable degree of selectivity

especially against other members of the mTOR pathway (IGF-1R, PDK1, PI3K β) although overall **4c** appeared slightly better in its profile with ≥ 5 -fold selectivity for mTOR over the kinases evaluated.

Compounds **3c** and **4c** were also profiled in cells for mechanistic effects on T37/46 p4E-BP1 and S473 pAkt.¹³ Despite their modest biochemical potency, both **3c** and **4c** completely inhibited T37/46 4E-BP1 phosphorylation in MDA-MB-231 cells with IC_{50} values of 7.4 and 7.8 μM , respectively. In contrast, rapamycin only demonstrated a maximal inhibition of 40% at 20 μM . Additionally, both agents inhibited S473 pAkt in BT-20 cells with IC_{50} values of 1.26 and 1.38 μM , respectively, indicative of inhibition of mTORC2. Rapamycin had no effect on inhibition of S473 pAkt at 20 μM . Functionally, both compounds demonstrated antiproliferative effects in MDA-MB-231 cells with IC_{50} values of 7.4 and 9.3 μM ,

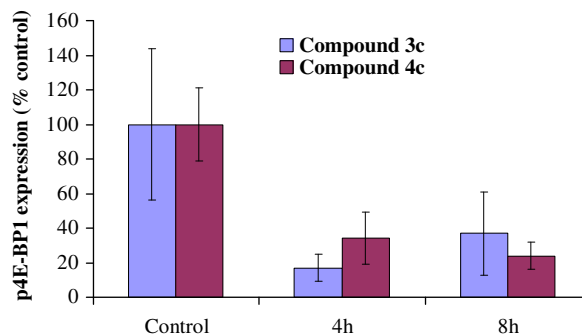


Figure 4. Pharmacodynamic inhibition of T37/46 4E-BP1 phosphorylation in MDA-MB-231 xenograft following oral dosing.

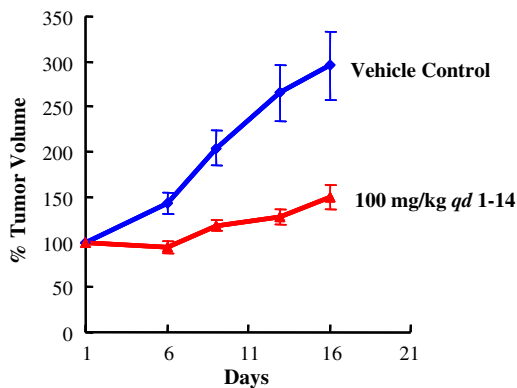


Figure 5. Tumor growth inhibition of compound **4c** in MDA-MB-231 xenograft.

respectively, commensurate with the mechanistic data and suggesting that these phenotypic effects were target mediated. Rapamycin was unable to inhibit any proliferation in this cell line ($IC_{50} > 50 \mu M$).

In addition to moderate ERs, both agents exhibited good permeability (PAMPA > 250 nm/s) and solubility ($> 100 \mu M$ at pH 7.4) and so were progressed to mouse PK studies. As shown in Table 8, both agents demonstrated high plasma exposures, as well as low clearance and good bioavailability on oral dosing at 20 mg/kg.

Despite the modest cell potencies of these compounds, the exposures obtained on oral dosing were sufficient to evaluate the potential of these agents to exert pharmacodynamic effects in vivo. To compensate for plasma protein binding effects (90.3% and 88.1% for **3c** and **4c**, respectively) these agents were dosed at 100 mg/kg to CD-1 nude mice bearing MDA-MB-231 xenografts. As shown in Figure 4, both agents were able to effect significant inhibition of 4E-BP1 phosphorylation at 4 and 8 h.

In order to assess whether such mechanistic target inhibition in vivo was sufficient to drive an associated functional effect, compound **4c** was dosed orally for 14 days at 100 mg/kg qd to CD-1 nude mice bearing subcutaneous MDA-MB-231 xenografts. The agent was well tolerated (body weight loss $\leq 2\%$) and this dose indeed resulted in 94% tumor growth inhibition (Fig. 5).¹⁴

In summary, our efforts towards the discovery of dual mTORC1/2 inhibitors led to the identification of a series of 1,3-disubstituted imidazo[1,5-*a*]pyrazin-8-amines. Optimization of the 1- and 3-substituents resulted in compounds **3c** and **4c** that combined sub-micromolar mTOR biochemical potency, mechanistic and phenotypic effects in a rapamycin resistant cell line, and in vitro metabolic stability. Both agents also exhibited emerging kinase selectivity and excellent pharmacokinetics on oral dosing. In particular, proof-of-concept compound **4c** was identified that demonstrated in vivo target inhibition in xenografts, with commensurate and significant inhibition of tumor growth in this tumor line and thereby establishing the viability of this series as orally efficacious dual mTORC1/2 inhibitors. Further optimization of compound **4c** in terms of potency, selectivity and general in vivo properties, leading to the discovery of the clinical mTORC1/2 agent OSI-027 will be described in future communications.

Acknowledgements

We would like to thank Mr. Paul Maresca and Ms. Maureen Brooks for developing and running the HTS, Mr. Peter Meyn, Ms. Jo Dunseath and Mr. Roy Turton for in vitro ADMET support,

and Ms. Viorica Lazarescu and Dr. Minghui Wang for analytical support.

Additionally we would like to recognize Dr. Arno G. Steinig, Dr. An-Hu Li and Mr. Anthony Nigro from the OSI IGF-1R team by whom some of the chemical seeds and intermediates used in this work were generated.^{11,12}

References and notes

- (a) Faivre, S.; Kroemer, G.; Raymond, E. *Nat. Rev. Drug Disc.* **2006**, *5*, 671; (b) Guertin, D. A.; Sabatini, D. M. *Cancer Cell* **2007**, *12*, 9; (c) Wullschlegler, S.; Loewith, R.; Hall, M. N. *Cell* **2006**, *124*, 471; (d) Chiang, G. G.; Abraham, R. T. *Trends Mol. Med.* **2007**, *13*, 433; (e) Meric-Bernstam, F.; Gonzalez-Angulo, A. M. *J. Clin. Oncol.* **2009**, *27*, 2278.
- (a) Laplante, M.; Sabatini, D. M. *J. Cell Sci.* **2009**, *122*, 3589; (b) Proud, C. G. *Biochem. Soc. Trans.* **2009**, *37*, 227.
- (a) Loewith, R.; Jacinto, E.; Wullschlegler, S.; Lorberg, A.; Crespo, J. L.; Bonenfant, D.; Oppliger, W.; Jenoe, P.; Hall, M. N. *Mol. Cell* **2002**, *10*, 457; (b) Hay, N.; Sonenberg, N. *Genes Dev.* **2004**, *18*, 1926.
- (a) Sarbassov, D. D.; Guertin, D. A.; Ali, S. M.; Sabatini, D. M. *Science* **2005**, *307*, 1098; (b) Engelman, J. A. *Nat. Rev. Cancer* **2009**, *9*, 550.
- O'Reilly, K. E.; Rojo, F.; She, Q.-B.; Solit, D.; Mills, G. B.; Smith, D.; Lane, H.; Hofmann, F.; Hicklin, D. J.; Ludwig, D. L.; Baselga, J.; Rosen, N. *Cancer Res.* **2006**, *66*, 1500.
- (a) Bhagwat, S. V.; Crew, A. P.; Gokhale, P. C.; Yao, Y.; Kahler, J.; Arnold, L. D.; Epstein, D. M.; Wild, R.; Pachter, J. A. *Abstr. Am. Assoc. Cancer Res.* **2009**, *100*, 3711; (b) Bhagwat, S. V.; Crew, A. P.; Gokhale, P. C.; Yao, Y.; Kahler, J.; Epstein, D. M.; Wild, R.; Pachter, J. A. *Abstr. Am. Assoc. Cancer Res.* **2010**, *101*, 4487; (c) Choo, A. Y.; Yoon, S.-O.; Kim, S. G.; Roux, P. P.; Blenis, J. *PNAS* **2008**, *105*, 17414.
- (a) Raynaud, F. I.; Eccles, S.; Clarke, P. A.; Hayes, A.; Nutley, B.; Alix, S.; Henley, A.; Di-Stefano, F.; Ahmad, Z.; Guillard, S.; Bjerke, L. M.; Kelland, L.; Valenti, M.; Patterson, L.; Gowan, S.; Brandon, A. H.; Hayakawa, M.; Kaizawa, H.; Koizumi, T.; Ohishi, T.; Patel, S.; Saghir, N.; Parker, P.; Waterfield, M.; Workman, P. *Cancer Res.* **2007**, *67*, 5840; (b) Maira, S.-M.; Stauffer, F.; Brueggen, J.; Furet, P.; Schnell, C.; Fritsch, C.; Brachmann, S.; Chène, P.; Pover, A. D.; Schoemaker, K.; Fabbro, D.; Gabriel, D.; Simonen, M.; Murphy, L.; Finan, P.; Sellers, W.; Garcia-Echeverria, C. *Mol. Cancer Ther.* **2008**, *7*, 1851; (c) Chresta, C. M.; Davies, B. R.; Hickson, I.; Harding, T.; Cosulich, S.; Critchlow, S. E.; Vincent, J. P.; Ellston, R.; Jones, D.; Sini, P.; James, D.; Howard, Z.; Dudley, P.; Hughes, G.; Smith, L.; Maguire, S.; Hummersone, M.; Malagu, K.; Menear, K.; Jenkins, R.; Jacobsen, M.; Smith, G. C. M.; Guichard, S.; Pass, M. *Cancer Res.* **2010**, *70*, 288; (d) Thoreen, C. C.; Kang, S. A.; Chang, J. W.; Liu, Q.; Zhang, J.; Gao, Y.; Reichling, L. J.; Sim, T.; Sabatini, D. M.; Gray, N. S. *J. Biol. Chem.* **2009**, *284*, 8023; (e) Apse, B.; Blair, J. A.; Gonzalez, B.; Nazif, T. M.; Feldman, M. E.; Aizenstein, B.; Hoffman, R.; Williams, R. L.; Shokat, K. M.; Knight, Z. A. *Nat. Chem. Biol.* **2008**, *4*, 691; (f) Yu, K.; Shi, C.; Toral-Barza, L.; Lucas, J.; Shor, B.; Kim, J. E.; Zhang, W.-G.; Mahoney, R.; Gaydos, C.; Tardio, L.; Kim, S. K.; Conant, R.; Curran, K.; Kaplan, J.; Verheijen, J.; Ayralkaloustian, S.; Mansour, T. S.; Abraham, R. T.; Zask, A.; Gibbons, J. J. *Cancer Res.* **2010**, *70*, 621; (g) Jessen, K.; Wang, S.; Kessler, L.; Guo, X.; Kucharski, J.; Staunton, J.; Lan, L.; Elia, M.; Stewart, J.; Bown, J.; Li, L. *Mol. Cancer Ther.* **2009**, *8*, B148.
- Bhagwat, S. V.; Crew, A. P. *Curr. Opin. Invest. Drugs* **2010**, *11*, 638.
- Bhagwat, S. V.; Kahler, J.; Yao, Y.; Maresca, P.; Brooks, M.; Crew, A.; Boisclair, M.; Pachter, J. A. *Assay Drug Dev. Technol.* **2009**, *7*, 471.
- Mulvihill, M. J.; Cooke, A.; Rosenfeld-Franklin, M.; Buck, E.; Foreman, K.; Landfair, D.; O'Connor, M.; Pirrit, C.; Sun, Y.; Yao, Y.; Arnold, L. D.; Gibson, N. W.; Ji, Q. S. *Future Med. Chem.* **2009**, *1*, 1153.
- Mulvihill, M. J.; Ji, Q.-S.; Coate, H. R.; Cooke, A.; Dong, H.; Feng, L.; Foreman, K.; Rosenfeld-Franklin, M.; Honda, A.; Mak, G.; Mulvihill, K. M.; Nigro, A. I.; O'Connor, M.; Pirrit, C.; Steinig, A. G.; Siu, K.; Stolz, K. M.; Sun, Y.; Tavares, P. A. R.; Yao, Y.; Gibson, N. W. *Bioorg. Med. Chem.* **2008**, *16*, 1359.
- Mulvihill, M. J.; Ji, Q.-S.; Werner, D.; Beck, P.; Cesario, C.; Cooke, A.; Cox, M.; Crew, A.; Dong, H.; Feng, L.; Foreman, K. W.; Mak, G.; Nigro, A.; O'Connor, M.; Saroglou, L.; Stolz, K. M.; Sujka, I.; Volk, B.; Weng, Q.; Wilkes, R. *Bioorg. Med. Chem. Lett.* **2007**, *17*, 1091.
- Falcon, B. L.; Barr, S.; Gokhale, P. C.; Chou, J.; Fogarty, J.; Depeille, P.; Miglarese, M.; Epstein, D. M.; McDonald, D. M. *Cancer Res.* **2011**, *71*, 1.
- Female *nu/nu* CD-1 mice were used in the xenograft studies. To assess anti-tumor efficacy, MDA-MB-231 cells were implanted into the mammary fat pad. Tumors were allowed to establish to $200 \pm 50 \text{mm}^3$ before randomization into treatment groups. Tumor volumes were determined twice weekly from caliper measurements by $V = (\text{length} \times \text{width}^2)/2$. Tumor growth inhibition (TGI) was determined by $\%TGI = \{1 - [(T_t/T_0)/(C_t/C_0)]/1 - [C_t/C_0]\} \times 100$, where T_t = tumor volume of treated animal \times at time t , T_0 = tumor volume of treated animal \times at time 0, C_t = median tumor volume of control group at time t , and C_0 = median tumor volume of control group at time 0. Mean %TGI was calculated for the entire dosing period for each group. Significant anti-tumor activity is defined as mean %TGI $> 50\%$.